Sensors & Actuators: A. Physical 355 (2023) 114303

Contents lists available at ScienceDirect

Sensors and Actuators: A. Physical

journal homepage: www.journals.elsevier.com/sensors-and-actuators-a-physical

Energy harvesting using a magnetostrictive transducer based on switching control

An Li [a,*], Keiju Goto [a], Yuusuke Kobayashi [a], Yushin Hara [a], Yu Jia [b], Yu Shi [c], Constantinos Soutis [d], Hiroki Kurita [e], Fumio Narita [e], Keisuke Otsuka [a], Kanjuro Makihara [a,*]

[a] Department of Aerospace Engineering, Tohoku University, Sendai, Japan
[b] College of Engineering and Physical Sciences, Aston University, Birmingham, UK
[c] Department of Physical, Mathematical and Engineering Sciences, University of Chester, Chester, UK
[d] Aerospace Research Institute, University of Manchester, Manchester, UK
[e] Department of Frontier Sciences for Advanced Environment, Tohoku University, Sendai, Japan

ARTICLE INFO

Keywords:
Magnetostrictive materials
Energy harvesting
Switching control

ABSTRACT

In this work, a switching control energy harvesting method using magnetostrictive materials is proposed. By combining a magnetostrictive material, an electric circuit, and an electronic switch, large-scale kinetic to electrical energy conversion can be achieved. The magnetostrictive material, magnet bias, and coils constitute an energy transducer, called a magnetostrictive transducer. The electronic switch strategically controls the switching of the circuit state according to an input switching signal. Using numerical simulations, we optimised the parameters and validated the harvesting performance with experimental measurements using a 3.75 m vibrated cantilever truss structure. In 20.0 s, the proposed method achieved an electrical energy of approximately 45 μJ, which is seven times more than that of the conventional passive method.

1. Introduction

1.1. Background

Recently, wireless sensor networks (WSNs) [1] and Internet of Things (IoTs) [2] have attracted considerable attention and are being rapidly adopted in various fields. Energy harvesting is a promising technique that can produce renewable and clean electrical energy. Roadways and bridges are major infrastructures involved in daily life, and the movement of people and vehicles constantly affects these infrastructures through structural vibrations. The energy harvesting technique used for such systems [3] is schematically shown in Fig. 1. The vibration generated from moving transportation systems can provide a renewable and sustainable energy source that can potentially power structural health monitoring sensors.

Kinetic to electrical energy conversion can be achieved using various smart materials, including piezoelectric materials [4,5], dielectric elastomers [6], shape memory alloys [7], electrorheological fluids [8], magnetorheological fluids [9], magneto rheological elastomers [10,11], and magnetostrictive materials [12,13].

The energy harvesting method used in piezoelectric materials has been widely studied [14]. Lombardi and Lallart [15] proposed a synchronous electric charge and induced current extraction (SECICE) technique that can significantly increase output power, particularly for low-coupled or highly damped systems. For switching control to amplify energy harvesting, synchronised switch harvesting on an inductor (SSHI) has been proposed to control switch devices according to vibration displacements [16]. Jia and Seshia [17] presented a power optimisation design for piezoelectric cantilever vibration energy harvesters based on experimentally validated analytical and numerical analysis. Hara et al. [18–20] developed a self-sensing estimation method for switching control energy harvesters based on the SSHI method and proposed novel switching strategies for enhancing energy harvesting by addressing the vibration suppression effect. However, piezoelectric materials mainly comprise brittle ceramics, which may be unsuitable for complex or extreme environments. Hence, magnetostrictive materials have gained attention in recent years; they are a type of smart material comprised primarily of iron and rare-Earth elements, such as Terfenol-D (Tb-Dy-Fe), Fe-Co alloys, and Galfenol ($Fe_{81.4}Ga_{18.6}$) [21]. Because these materials are iron alloys, they have high mechanical strength and workability, which make them suitable for various complex environments.

Magnetostrictive materials can be used for conversion between

* Corresponding authors.
E-mail addresses: li.an.r3@dc.tohoku.ac.jp (A. Li), kanjuro.makihara.e3@tohoku.ac.jp (K. Makihara).

https://doi.org/10.1016/j.sna.2023.114303
Received 21 November 2022; Received in revised form 19 February 2023; Accepted 10 March 2023
Available online 14 March 2023

Nomenclature

b_m:	magnetostriction coefficient of magnetostrictive materials [V·s/m = N/A]
$\mathbf{B}_m$:	magnetostriction coefficient matrix
C_i:	capacitance of inversion capacitor [F]
C_h:	capacitance of harvesting capacitor [F]
CPCS:	current peak control strategy
D:	damping coefficient of structure [N·s/m]
E_h:	harvested electrical energy [J]
$\mathbf{f}_{ext}$:	multiple external force vector
F_m:	external force of magnetostrictive transducer [N]
I:	current [A]
I:	induced current vector of magnetostrictive transducers
k_m^I:	stiffness of magnetostrictive transducer at constant current [N/m]
k_{ti}:	stiffness of i-th bar member.
K:	constant-current stiffness matrix of structure
$L_m^{\dot{S}}$:	inductance of magnetostrictive transducer at constant velocity [H]
M:	mass matrix of structure
P_i:	axial force applied to i-th bar member [N]
Q_i:	charge of inversion capacitor [C]
Q_h:	charge of harvesting capacitor [C]
R_0:	internal resistance of coil [Ω]
T:	kinetic energy [J]
u:	elongation of magnetostrictive materials
V_m:	induced voltage of magnetostrictive transducer [V]
V_i:	voltage of C_i [V]
V_h:	harvested voltage [V]
VPCS:	velocity peak control strategy
W:	potential energy [J]
x:	displacement of structure [m]
x:	position coordinates of each node
ζ_e:	damping coefficient of inductor-capacitor electrical oscillation
ω_e:	frequency of inductor-capacitor electrical oscillation
Δt:	time difference [s]

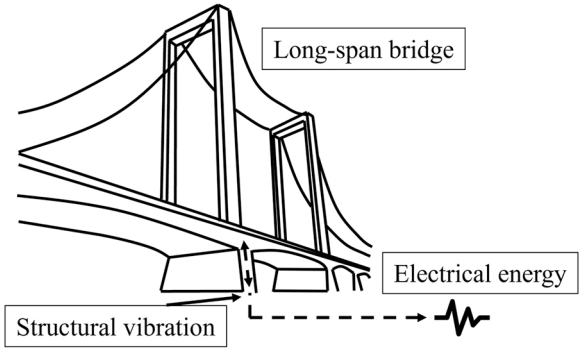

Fig. 1. Schematic of energy harvesting used in roadways and bridges [3].

kinetic and magnetic energy, which is referred to as the Villari-Joule effect [12]. The Joule effect is a property of ferromagnetic materials that causes them to generate a mechanical strain when subjected to a magnetic field. Meanwhile, the Villari effect is a property of magnetostrictive materials that causes them to become magnetically susceptible when subjected to mechanical stress. Magnetostrictive materials are typically used to design sensors and actuators [22–24]. Viola et al. [25] proposed a power generator using Terfenol-D for energy harvesting from traffic vibrations and experimentally validated this system. Zucca et al. [26] analysed the quantities that influence the performance of a direct force transducer based on Terfenol-D. The power generated by the transducer has a complex dependence on the coil characteristics, type of permanent magnets used, and mechanical excitation characteristics. Mori et al. [27] constructed a giant magnetostrictive cantilever with a Terfenol-D layer, stainless steel layer, and movable proof mass designed to automatically adjust the resonant frequency to match the external vibration frequency in real-time. Researchers focused on the use of Galfenol and found that the magnetostrictive effect of Galfenol was optimal when the composition ratio of Ga was approximately 20% [28–30]. They also clarified the influence of an external magnetic field on the magnetostrictive effect by focusing on the elastic modulus of the magnetostrictive material under the influence of an optimal external magnetic field. Kita et al. [31] developed a high-power magnetostrictive vibration power generator for battery-free wireless electronics based on a cantilever parallel beam structure consisting of coil-wound Galfenol and stainless plates with a permanent magnet for bias. Ueno [32] proposed a simple, robust, and highly sensitive vibration power generation device based on the unimorph of an Fe-Ga plate and U-shaped frame. Li et al. [33] presented an energy harvester employing a cantilever beam and magnetostrictive/piezoelectric laminate transducer to transform rotational energy into electrical energy. Li et al. [34] proposed a ferro-nickel (Fe-Ni)/PZT H-type fork magnetoelectric composite structure with a high quality value and energy management circuit for harvesting. Iannone et al. [35] connected the magnetostrictive harvester to an AC-DC boost converter. Based on the simulation results, the proposed circuit was proven to increase more output voltage than that induced by the magnetostrictive harvester. Clemente et al. [36] presented the experimental verification of an AC-DC boost converter driven with a real-time operating Arduino board.

1.2. Objectives

Combining energy harvesting control and piezoelectric materials has attracted considerable research interest. Correspondingly, improvements in magnetostrictive material properties have been a research focus, while several studies have focused on energy harvesting control to achieve more efficient harvesting performance. Conventional studies typically utilise a half rectifier circuit to passively harvest electrical energy.

The objective of this study is to propose a novel energy harvesting method using a magnetostrictive transducer. The method differs from that of conventional studies because strategical switching between multiple electrical systems is utilised. This results in a better energy harvesting performance because the properties of the raw materials used are not altered, which is achieved by combining resistor-inductor (RL) and resistor-inductor-capacitor (RLC) circuits with a magnetostrictive transducer. As the state of the circuit changes, the electrical energy temporarily stored in the coils and capacitor is amplified, thereby amplifying the harvested electrical energy. Subsequently, two control strategies that can be synchronised using mechanical vibrations to switch between the circuit states are discussed.

The proposed switching control strategies are applied to a truss structure to simulate flexible infrastructure. The harvesting performance of the proposed method is predicted by numerical simulations and validated by experimental measurements.

2. Theoretical analysis, circuit design, and switching control strategies

2.1. Equation of magnetostrictive transducer

The overall strength when the transducer is embedded in the structure must be considered. Although the magnetostriction of Terfenol-D is the largest, it cannot play a load-bearing role owing to its fragility. While ensuring relatively large magnetostriction, the mechanical strength of Galfenol is higher than that of Terfenol-D. Considering the combination with target structures, we assumed that the magnetostrictive materials and other components exhibit similar Young's modulus. Hence, Galfenol ($Fe_{81.4}Ga_{18.6}$) was selected as the magnetostrictive material.

The magnetostrictive transducer used consists of Galfenol, coils, and neodymium magnets, as shown in Fig. 2(a). Magnetostrictive transducers are an electromechanically coupled system, and their fundamental equations can be derived as

$$F_m = k_m^I u - b_m I, \tag{1}$$

$$V_m = -b_m \dot{u} - L_m^{\dot{S}} \dot{I} - R_0 I, \tag{2}$$

where k_m^I is the stiffness of the magnetostrictive transducer at constant current, $L_m^{\dot{S}}$ is the inductance of the magnetostrictive transducer at constant velocity, b_m represents the magnetostriction coefficient of the magnetostrictive transducer, while F_m, V_m, u, and I represent the external force acting on the magnetostrictive transducer, induced voltage of the magnetostrictive transducer, elongation of the magnetostrictive material, and current, respectively. Therefore, by using a magnetostrictive transducer, the kinetic energy from vibrations can be converted into electrical energy. Magnetostrictive transducers behave as a voltage source in tandem with the coils and an internal resistor R_0. Fig. 2(b) shows the schematic of an electrical model for such systems.

2.2. Proposed control circuit and mechanism

Fig. 3 illustrates a conventional passive harvesting system in which the magnetostrictive transducer is assembled in tandem with a diode to form a half rectifier passive circuit. Because the conventional passive harvesting system using a diode only aims to rectify the AC voltage V_m to a DC voltage, the maximum value of the DC voltage will not exceed the amplitude of V_m. Hence, we consider that this diode-based passive harvesting method will not amplify the harvested energy. However, this passive method cannot amplify harvested energy from the magnetostrictive transducer.

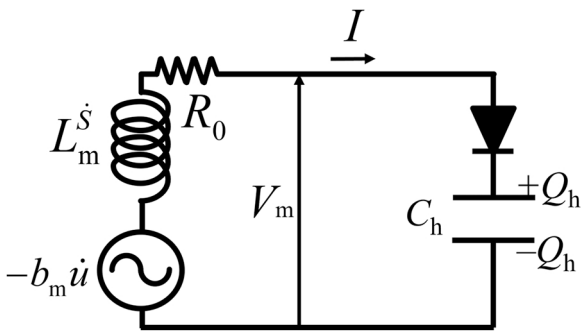

Fig. 3. Electrical model of magnetostrictive transducer assembled with half rectifier passive circuit: $L_m^{\dot{S}}$, inductance of magnetostrictive transducer at constant velocity; b_m, magnetostriction coefficient of magnetostrictive transducer; V_m, induced voltage of magnetostrictive transducer; u, elongation of the magnetostrictive material; I, current; R_0, internal resistor; C_h, harvesting capacitor; Q_h, charge of harvesting capacitor.

The harvesting performance of magnetostrictive transducers is improved by introducing the circuit shown in Fig. 4, which consists of a magnetostrictive transducer, two capacitors (C_i, C_h), two diodes, and an electronic switch. Here, $L_m^{\dot{S}}$ is combined with the inversion capacitor C_i to form a high-frequency inductor-capacitor (LC) electrical oscillation. C_h is the harvesting capacitor that accumulates electrical energy. The electronic switch is selected between points X and Y. Fig. 5 shows each

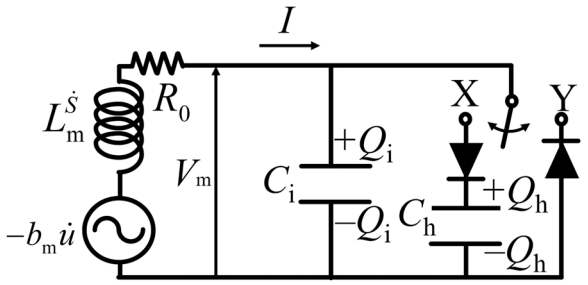

Fig. 4. Proposed circuit assembly for magnetostrictive transducer with electronic switch: $L_m^{\dot{S}}$, inductance of magnetostrictive transducer at constant velocity; b_m, magnetostriction coefficient of magnetostrictive transducer; V_m, induced voltage of magnetostrictive transducer; u, elongation of the magnetostrictive material; I, current; R_0, internal resistor; C_h, harvesting capacitor; Q_h, charge of harvesting capacitor; Q_i, charge of inversion capacitor.

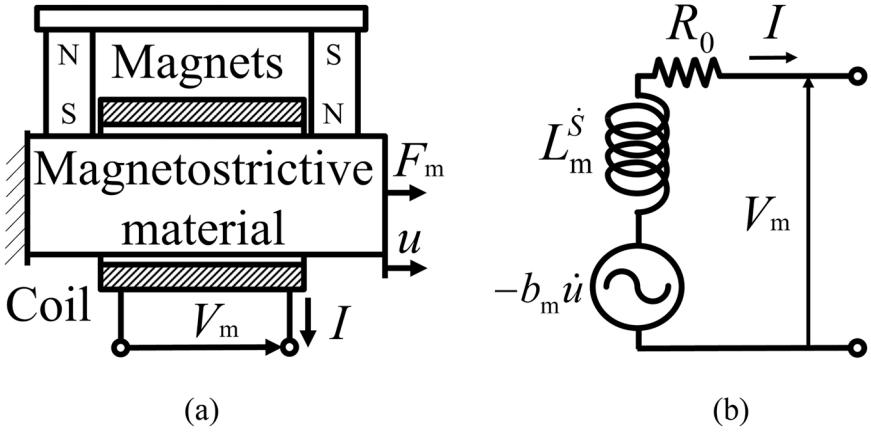

Fig. 2. Schematic of magnetostrictive transducer and corresponding electrical circuit: $L_m^{\dot{S}}$, inductance of magnetostrictive transducer at constant velocity; b_m, magnetostriction coefficient of magnetostrictive transducer; F_m, external force acting on magnetostrictive transducer; V_m, induced voltage of magnetostrictive transducer; u, elongation of the magnetostrictive material; I, current; R_0, internal resistor.

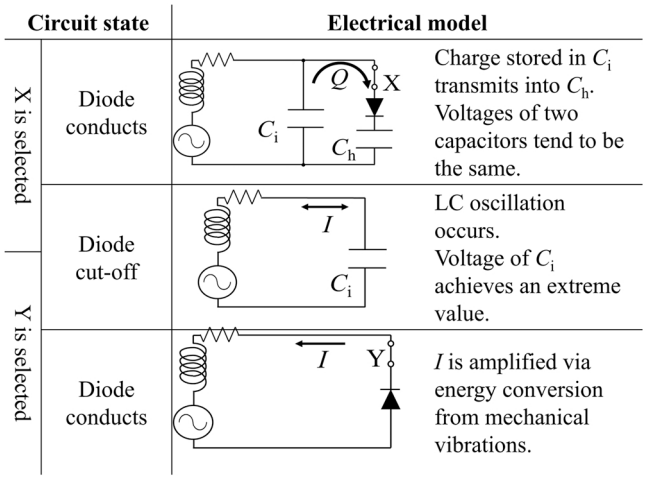

Fig. 5. Current and voltage mechanisms of proposed circuit: I, current; C_h, harvesting capacitor; C_i, inversion capacitor; Q, charge; LC, inductor-capacitor.

circuit state during the switching and energy harvesting processes. The elongation u is assumed to be a sinusoidal function described by $u = U\sin(\omega t+\gamma)$. The proposed circuit contains three circuit states: short, LC, and charge transfer.

When point X is selected, if the diode is conducting, the harvesting process can be divided into passive and charge transfer processes. When the passive process occurs, the circuit connected to the anode of the diode can be considered to be an open circuit, and the input voltage of the diode V_D can be described as

$$V_D = -b_m\dot{u} - L_m^{\dot{S}}\dot{I} - R_0 I. \tag{3}$$

Because the magnetostrictive transducer is opened, I decreases to zero. When $I = 0$, V_D approaches $-b_m\dot{u}$. The harvested voltage of C_h becomes infinitely close to V_D when the diodes are assumed to be ideal. Therefore, the passive method has a limit for energy harvesting.

When the charge transfer occurs, the charge stored in C_i transfers into C_h due to a potential difference. Increasing the potential difference between the two capacitors can increase the voltage of C_h. However, as in the passive process described above, the voltage of C_h cannot be larger than that of C_i.

When point Y is selected, the circuit connected in tandem forms a short circuit if the diode is conducting. The circuit equation can be described as

$$L_m^{\dot{S}}\dot{I} + R_0 I = -b_m\dot{u},\ Q_i/C_i = 0,\ \dot{Q}_h/C_h = 0, \tag{4}$$

where Q_i and Q_h are the charges of the inversion and harvesting capacitors, respectively. In this process, the electrical energy induced from the magnetostrictive transducer will increase with the structural vibration. I can be calculated as

$$I = -\exp\left(-\frac{R_0}{L_m^{\dot{S}}}t\right)\int\frac{b_m\dot{u}}{L_m^{\dot{S}}}\exp\left(\frac{R_0}{L_m^{\dot{S}}}t\right)dt. \tag{5}$$

where t is time. Because C_h and C_i are shorted, the harvesting process does not occur, and the electrical energy is temporarily stored in $L_m^{\dot{S}}$.

Regardless of the selected point, if the diode is not conducting, I flows through C_i. The LC electrical oscillation caused by $L_m^{\dot{S}}$ and C_i occurs. The circuit equation can be described as

$$L_m^{\dot{S}}\dot{I} + R_0 I + \frac{Q_i}{C_i} = -b_m\dot{u},\ \dot{Q}_h\Big/C_h = 0. \tag{6}$$

Eq. (6) can be rewritten as

$$L_m^{\dot{S}}\ddot{Q}_i + R_0\dot{Q}_i + \frac{Q_i}{C_i} = -b_m U\omega\cos(\omega t+\gamma),\ \dot{Q}_h\Big/C_h = 0. \tag{7}$$

The solution of Eq. (7) can be determined as

$$Q_i = A\exp(-\zeta_e\omega_e t)\sin\left(\omega_e\sqrt{1-\zeta_e^2}\,t+\theta-\lambda\right) + \frac{b_m U}{L_m\sqrt{(\omega_e{}^2-\omega^2)^2+4\omega_e{}^2\omega^2\zeta_e^2}}\cos(\omega t+\gamma+\sigma), \tag{8}$$

where A and θ are constants determined by the initial conditions; ω_e and ζ_e represent the frequency and damping coefficient of LC electrical oscillation, respectively; and ω_e, ζ_e, λ, and σ can be defined as

$$\omega_e \equiv \frac{1}{\sqrt{L_m^{\dot{S}}C_i}},\ \zeta_e \equiv \frac{R_0}{2}\sqrt{\frac{C_i}{L_m^{\dot{S}}}},\ \lambda \equiv \tan^{-1}\left(\frac{\sqrt{1-\zeta_e{}^2}}{\zeta_e}\right),\ \sigma \equiv \tan^{-1}\left(\frac{2\omega_e\omega\zeta_e}{\omega_e{}^2-\omega^2}\right) \tag{9}$$

The voltage of C_i can be summarised as

$$V_i = \frac{A\exp(-\zeta_e\omega_e t)}{C_i}\sin\left(\omega_e\sqrt{1-\zeta_e^2}\,t-\theta\right) + \frac{b_m U}{C_i L_m\sqrt{(\omega_e{}^2-\omega^2)^2+4\omega_e{}^2\omega^2\zeta_e^2}}\cos(\omega t+\gamma+\sigma). \tag{10}$$

V_i is determined by the initial conditions of the circuit state before switching. Therefore, the time associated with changing circuit states determines the maximum V_i value. Eq. (10) comprises electrical and mechanical terms. The first term refers to the voltage of LC electrical free oscillation, while the second term refers to the induced voltage from structural vibration. Because the amplitude of the first term is related to time t, the amplitude is considerably affected by the exponential function. In contrast, the amplitude of the second term is constant. Furthermore, C_i is selected as an extremely small value to ensure that the LC oscillation frequency is considerably higher than the structural vibration frequency. During the LC oscillation, the first term is more active with time t. Therefore, this term has a greater effect on V_i.

2.3. Theoretical control strategies

In conventional piezoelectric energy harvesting technologies, LC oscillation is used to amplify the induced voltage converted from

mechanical vibrations. These technologies have associated switching control strategies for synchronising electromechanical systems. These conventional strategies for the piezoelectric elements work by detecting the peaks of the mechanical displacement or electrical charge. In the case of magnetostrictive transducers, we focused on the induced current since the magnetostrictive transducer was assimilated into the inductor as shown in Fig. 2(b). Because the induced current is related to the strain velocity, as described in Eq. (2), the control strategies for the magnetostrictive transducer should also focus on the strain velocity or the induced current. Herein, two switching control strategies are developed.

Within the mechanical system, when the vibration velocity reaches the maximum value, the kinetic energy is high because the magnetostrictive transducer induces the most electrical energy when the kinetic energy of the mechanical system is maximised. Hence, the velocity peak control strategy (VPCS) is proposed. VPCS aims to switch between connection points when the structural vibration velocity is maximised. To realise VPCS, the velocity of the structural vibration is required.

Within the electrical system, when the induced current reaches a maximum value, the harvested energy through the electrical circuit is high because internal resistance is inevitable in an actual electrical circuit. The composition of the internal resistance and inductance of the magnetostrictive transducer cause a phase shift between the velocity and induced current. Hence, the current peak control strategy (CPCS) is also proposed. CPCS aims to switch between connection points when the induced current is maximised. To realise CPCS, the induced current of the electrical circuit is required.

2.4. Applicable control strategies using truss displacement

Using a single-mode vibration application environment, we confirm that the acceleration of the elongation and displacement of the structure maintain the same phase. Considering the compositions of the magnetostrictive transducer and truss structure, we chose the displacement of the structure to predict the velocity peak. Therefore, we proposed VPCS as

[VPCS]: When $x > 0$, point Y should be selected.
When $x < 0$, point X should be selected.

Here, x is the displacement of the structure.

Regarding CPCS, we need to detect the induced current of the electrical circuit. However, due to noise and LC electrical oscillation, the current peak is difficult to detect. Because the initial magnetic field is considerably larger than the magnetic field changing due to strain vibrations in our experimental environment, we assumed that this magnetostrictive transducer shows a linear relationship between the magnetic field and strain. Furthermore, under this initial magnetic field, the inductance and internal resistance maintain constant values. The phase difference between the vibration velocity and induced current is determined by the inductance and resistance. Hence, we designed CPCS based on VPCS and the phase difference between the vibration velocity and circuit current. When we only consider the case of the first natural vibration mode, the current peak can be calculated by introducing a phase difference based on the vibration velocity; we propose the following method to simulate CPCS. An appropriate time based on the vibration velocity and induced current is proposed, which can be used to estimate the maximum current value by measuring the displacement value without measuring the current value, thereby realising the same switching signal at the induced current peak. Therefore, we proposed CPCS as:

[CPCS]: If $x(t_0) > 0$, when $t = t_0 + \Delta t$, point Y should be selected.
If $x(t_0) < 0$, when $t = t_0 + \Delta t$, point X should be selected.

Here, Δt is the time difference between the current and velocity peaks that can be calculated as follows. Upon substituting Eq. (8) into Eq. (7) and integrating, I can be calculated as

$$I = C_1 \exp\left(-\frac{R_0}{L_m^S}t\right) - \frac{\omega b_m U}{\sqrt{{R_0}^2 + \left(\omega L_m^S\right)^2}} \sin\left(\omega t + \gamma + \varphi\right), \tag{11}$$

where

$$\alpha \equiv \frac{R_0}{L_m^S},\ \varphi \equiv \tan^{-1}\left(\frac{\alpha}{\omega}\right) = \tan^{-1}\left(\frac{R_0}{\omega L_m^S}\right), \tag{12}$$

where C_1 is constant and φ is the phase difference between the strain and the induced current. Eq. (11) can be differentiated to give

$$\dot{I} = C_2 \exp\left(-\frac{R_0}{L_m^S}t\right) - \frac{\omega^2 b_m U}{\sqrt{{R_0}^2 + \left(\omega L_m^S\right)^2}} \sin\left(\omega t + \gamma + \varphi - \frac{\pi}{2}\right), \tag{13}$$

where C_2 is constant. Because under the first natural vibration mode, x and u are proportional and in phase, $\ddot{u}$ and x have the same phase relationship. Meanwhile, the sign judgement indices of CPCS and VPCS are opposite. From Eq. (13), we can derive that $\dot{I}$ and x have an opposite phase relationship. The phase difference between $\dot{I}$ and u is $\pi/2 - \varphi$, and Δt can be derived and defined as

$$\Delta t \equiv \frac{\pi}{2\omega} - \frac{1}{\omega}\tan^{-1}\left(\frac{R_0}{\omega L_m^S}\right). \tag{14}$$

By combining VPCS and Δt, CPCS can be realised by measuring the displacement and electrical parameters of the circuit. CPCS can then be rewritten as follows:

[CPCS]: If $x(t_0) > 0$, when $t = t_0 + \frac{\pi}{2\omega} - \frac{1}{\omega}\tan^{-1}\left(\frac{R_0}{\omega L_m^S}\right)$, point Y should be selected.
If $x(t_0) < 0$, when $t = t_0 + \frac{\pi}{2\omega} - \frac{1}{\omega}\tan^{-1}\left(\frac{R_0}{\omega L_m^S}\right)$, point X should be selected.

Fig. 6 shows the switching signals obtained using CPCS and VPCS. The switching signals maintain the same frequency as the structural vibration. The CPCS switching signal shows that when the induced current increases, point X is selected; otherwise, point Y is selected. The VPCS switching signal shows that when the displacement is negative, point X is selected; otherwise, point Y is selected.

3. Numerical simulation for each harvesting control strategy

To compare the harvesting performances of the control strategies, we simulated the vibration of the cantilevered 10-bay truss structure shown in Fig. 7. Here, x represents the displacement of the truss structure along the X-axis. The magnetostrictive transducer was attached to the base of the structure and replaced one bar member in the first bay. The modal damping ratio ζ_i of each vibration mode was determined as 9.7×10^{-3}. We analysed this system as a discrete structure and systematically constructed the equation of motion using the finite element method. The parameters of the numerical simulation are shown in Table 1. Each parameter was based on actual experimental setups. The excited vibration mode was the first natural bending vibration mode in the X-axis, and the excitation point was set at the fourth bay of the truss structure. The motion equation for the magnetostrictive transducer with the truss structure can be derived from Appendix A. All numerical simulations were conducted using MATLAB (MathWorks, Inc., USA).

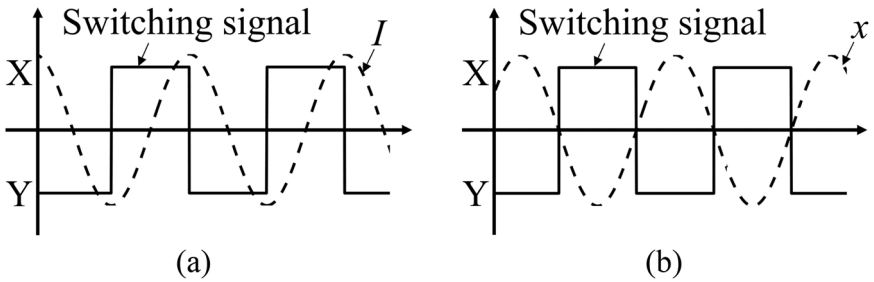

Fig. 6. Switching signals achieved using current peak control strategy (CPCS) and velocity peak control strategy (VPCS).

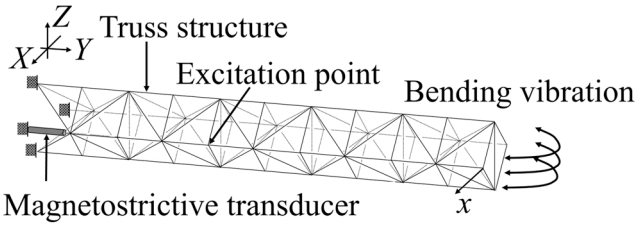

Fig. 7. Truss structure with magnetostrictive transducer.

Table 1
Parameters of numerical simulation.

Parameter	Value
Stiffness of bar member, k_t	1.99×10^6 N/m
Ordinary bar member length, l_o	3.80×10^{-1} m
Diagonal bar member length, l_d	5.40×10^{-1} m
Ordinary bar member mass, m_o	3.57×10^{-2} kg
Diagonal bar member mass, m_d	4.63×10^{-2} kg
Node mass, m_n	6.79×10^{-2} kg
Stiffness at constant current, k_m^I	1.60×10^7 N/m
Magnetostriction coefficient, b_m	1.15×10^2 N/A
Inductance at constant velocity, L_m^S	1.90×10^{-1} H
Inversion capacitance, C_i	1.00×10^{-6} F
Harvesting capacitance, C_h	1.00×10^{-3} F
Internal resistance, R_0	2.18×10^1 Ω
Time step	1.00×10^{-5} s

3.1. Harvesting processes and comparison between VPCS and CPCS

We simulated an excitation vibration acting on the truss structure. The motion and circuit equations were calculated using the Runge-Kutta fourth-order method. The initial values I_0 and x_0 were both zero. Because we intended to compare the harvesting performances of VPCS and CPCS, the passive method was performed until its harvested energy reached saturation. The simulation time was 20.0 s, during which the passive method was used for the first 10.0 s and the switching signal from 10.0 s to the end of the experiment. The frequency of the first natural vibration mode was 11.40 Hz.

Fig. 8 shows the time histories of the voltages of C_h (V_h) and C_i (V_i) obtained using CPCS. Within the first 10.0 s of the excitation, V_i maintained a zero-state because no LC electrical oscillations occurred. V_h reached a saturation value immediately because the half rectifier passive circuit was conducted. When switching started at 10.0 s, V_i rapidly increased due to the LC electrical oscillation; in particular, the amplitude peak of V_i far exceeded the saturation value of V_h achieved by the passive method in the previous stage. From the time histories of V_h obtained during switching, we confirmed that the proposed control strategies realised a higher voltage stored in C_h than the passive method. Fig. 8(b) shows the partial enlargements at 15.0 s, where V_i forms an oscillation due to the switching. When V_i is larger than V_h before the switching, the charge stored in C_i is transferred to C_h. Hence, we assume

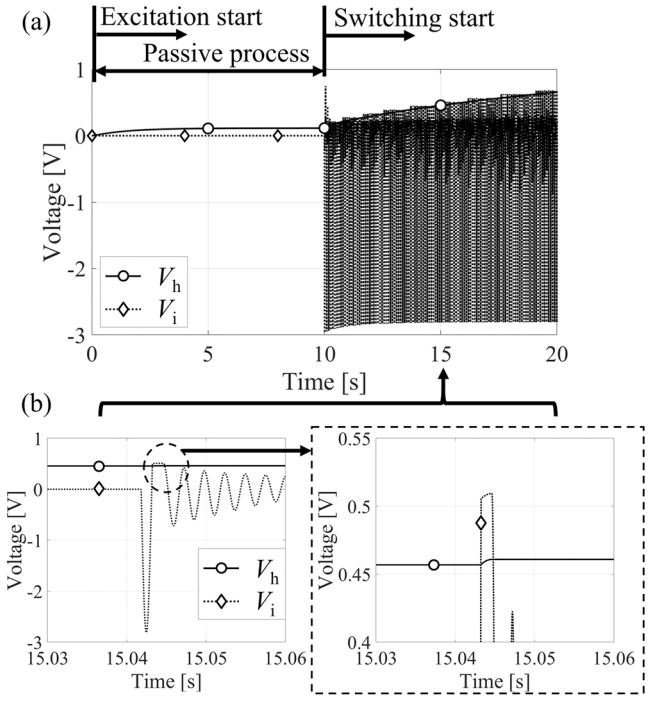

Fig. 8. (a) Time histories of voltages of inversion (V_i) and harvesting (V_h) capacitors, and (b) their partial enlargements at 15.0 s using current peak control strategy.

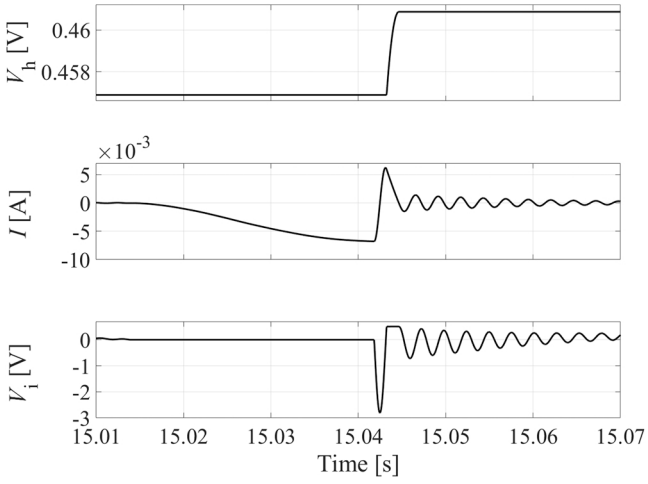

Fig. 9. Time histories of current (I) and voltage of inversion capacitor (V_i) during switching of connection points (partial enlargement).

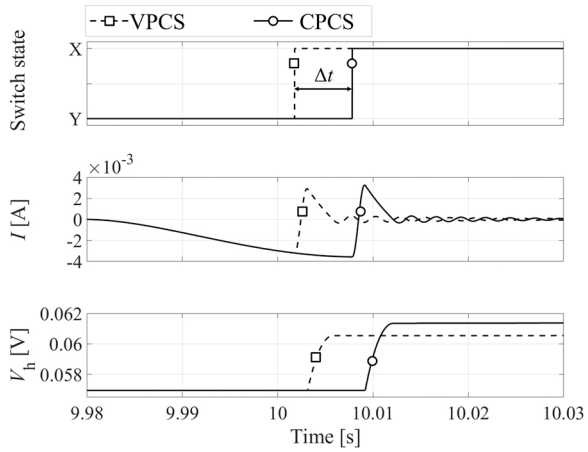

Fig. 10. Time histories of current (I) and voltage of harvesting capacitor (V_h) during switching using current peak control strategy (CPCS) and voltage peak control strategy (VPCS) (partial enlargement).

that the amplitude of the LC oscillation determines the final voltage value of V_h. Because the charge transfer is due to the electric potential difference between two capacitors, the acceleration of V_h reduces and continuously approaches the amplitude of the LC oscillation.

Fig. 9 shows the partial time histories of V_i, I, and V_h obtained using both switching control strategies. Because the switching signals changed the connection points, I inverted from negative to positive due to the LC electrical oscillation, and V_i reached a maximum value. C_h collected a certain amount of electrical energy at this stage, and V_h increased. Next, because of the circuit disconnection, LC electrical oscillation occurred, and I oscillated and decreased due to R_0 until the magnetostrictive transducer generated a negative current.

Fig. 10 shows the partial time histories of V_h, I, and the switching signals obtained using both switching control strategies. Because of the introduction of Δt, the current peaks of CPCS and VPCS tend to differ. When switching between connection points, I maintains a higher current state in CPCS than in VPCS. Because of the difference in the magnitude of the initial current at the moment of LC electrical oscillation, the electrical energy stored in the circuit at this time differs. A larger initial current results in a larger amplitude of the electrical energy oscillating in the circuit. Both LC electrical oscillations have the same period that is determined by C_i and L_m^S: the larger the amplitude of the LC electrical oscillation, the larger the rate of increase and decrease of V_i. The switching control strategy with larger increasing and decreasing rates indicates faster charge transport. Therefore, V_h of CPCS is higher than that of VPCS.

3.2. Harvesting performance of each strategy

As mentioned in section 3.1, CPCS can realise a more efficient energy harvesting performance than VPCS. We discuss VPCS, CPCS, and the conventional passive method in this section. To achieve VPCS, we only need the displacement of the 10th bay of the truss structure. Furthermore, by introducing a deliberate time difference based on VPCS, CPCS can be achieved. The harvested electrical energy E_h is introduced to measure the energy harvesting performance. E_h is defined as:

$$E_h \equiv \frac{1}{2} C_h V_h^2. \tag{15}$$

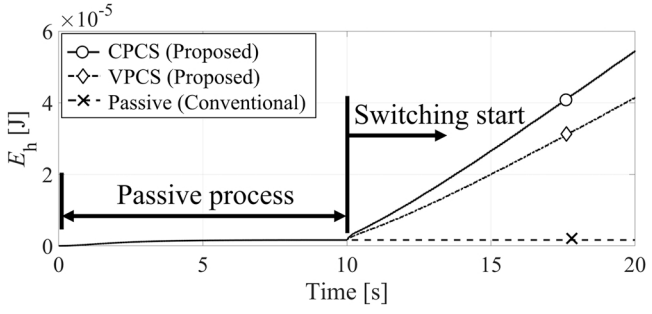

Fig. 11. Time histories of harvested electrical energy E_h using passive method, current peak control strategy (CPCS), and voltage peak control strategy (VPCS).

Table 2
Comparison of harvested energies from numerical simulations.

Harvesting method	Harvested energy [J]
Current peak control strategy (Proposed)	5.46×10^{-5}
Voltage peak control strategy (Proposed)	4.15×10^{-5}
Passive (Conventional)	1.63×10^{-6}

Fig. 11 shows the time histories of E_h using the passive method, CPCS, VPCS, and the conventional passive method. Over 20.0 s (with switching from 10.0 s), the two switching control strategies realise a significantly higher energy harvesting performance than the conventional passive method. Simultaneously, CPCS has a faster energy increase rate than VPCS, and the energy harvesting performance is also higher. The harvested energy obtained using each switching control strategy is summarised in Table 2. VPCS and CPCS realise 25 and 33 times more energy than the passive method, respectively. Furthermore, the difference achieved in the energy harvesting performance of the two switching control strategies implies that switching timing is a determining factor for energy harvesting performance.

3.3. Robustness analysis

Because of changes in material properties due to environmental changes, various unpredictable influences occur in actual harvesting circuits. Therefore, to investigate the robustness of the model error energy harvesting performance, we simulated energy harvesting using intentional model errors based on each harvesting method. For instance, parameters k_m^I and b_m are likely to cause differences between values designed under nominal conditions and values obtained in actual systems; therefore, they are valid parameters to manipulate for robustness validation.

Fig. 12 shows E_h obtained upon varying k_m^I. Because the exciting force is constant, each switching control strategy realised a higher energy harvesting performance than the passive strategy. Under all conditions, the energy harvesting performance decreases as k_m^I increases. This indicates that increasing k_m^I reduces the Villari-Joule effect, thereby reducing the energy harvesting performance of the system. Meanwhile, E_h decreases as $k_{m\_actual}^I / k_{m\_nominal}^I$ decreases. Here, $k_{m\_actual}^I$ and $k_{m\_nominal}^I$

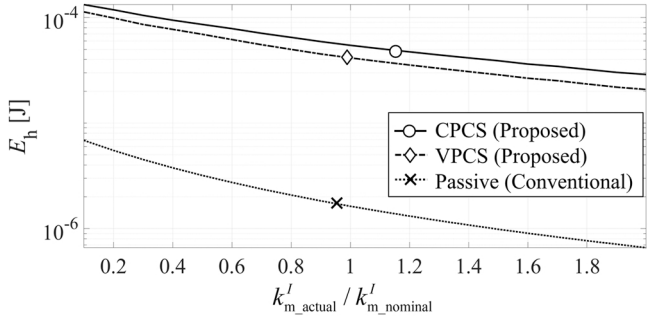

Fig. 12. Harvested electrical energy E_h using the passive method, current peak control strategy (CPCS), and voltage peak control strategy (VPCS) as a function of errors in the stiffness of the magnetostrictive transducer at constant current, k_m^I.

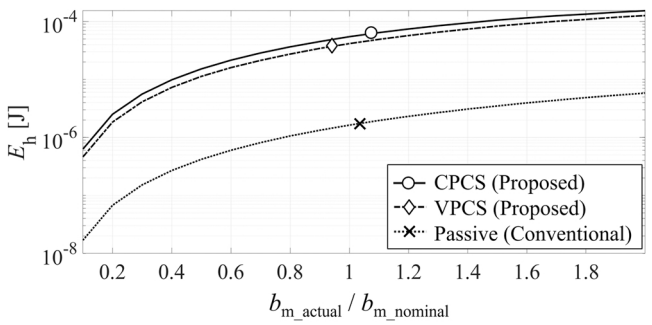

Fig. 13. Harvested electrical energy E_h using the passive method, current peak control strategy (CPCS), and voltage peak control strategy (VPCS) as a function of errors in the magnetostriction coefficient of the magnetostrictive transducer, b_m.

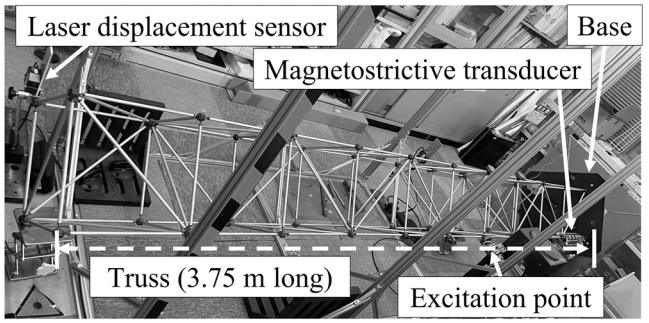

Fig. 14. Magnetostrictive transducer attached in truss structure.

represent the stiffness of the magnetostrictive transducer at a constant current obtained under actual and nominal conditions, respectively. The proposed switching control strategies exhibit similar robustness as the passive method.

Fig. 13 shows E_h obtained upon varying b_m. Because the exciting force is constant, each switching control strategy realises higher energy harvesting performance than the passive strategy. Under all conditions, the energy harvesting performance increases as b_m increases. Moreover, E_h increases as $b_{m\_actual}/b_{m\_nominal}$ increases. Here, b_{m_actual} and $b_{m\_nominal}$ represent the magnetostriction coefficient of the magnetostrictive transducer obtained under actual and nominal conditions, respectively.

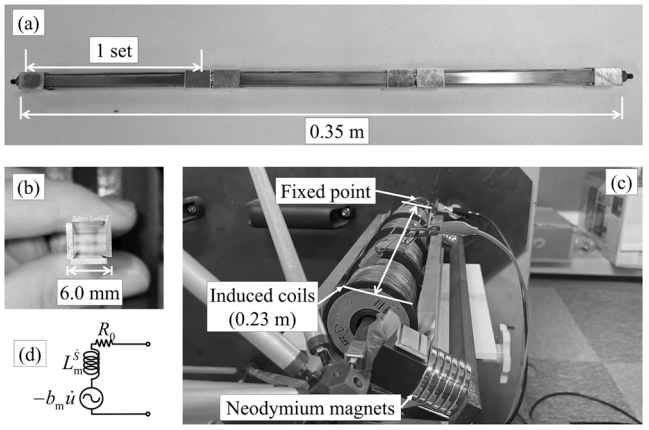

Fig. 15. (a) Top and (b) cross-sectional views of magnetostrictive materials. (c) Magnetostrictive transducer. (d) Electrical model of proposed magnetostrictive transducer: $L_m^{\dot{s}}$, inductance of magnetostrictive transducer at constant velocity; b_m, magnetostriction coefficient of magnetostrictive transducer; u, elongation of the magnetostrictive material; R_0, internal resistor.

From Eqs. (1) and (2), we observe that increasing b_m increases the induced voltage, such that the energy harvesting performance is also increased. The proposed switching control strategies exhibit similar robustness as the passive method.

4. Experimental validation of energy harvesting

4.1. Truss structure and equipment setup

To validate the energy harvesting performance of the proposed method in an actual structure, experiments were conducted using a cantilevered 10-bay truss structure with a length of 3.75 m and weight of 1.32×10^1 kg. Fig. 14 shows the experimental system. The dimensions of the bar members comprising the truss structure are summarised in Table 1. The bar members were connected by iron nodes. The truss structure was fixed on a base (end support). Two strings were used to counteract gravity such that the truss structure remained straight in the horizontal direction.

The magnetostrictive transducer replaced one ordinary bar member located at the first bay and connected to the fixed end support of the truss structure. Fig. 15 shows the magnetostrictive transducer used. The magnetostrictive material consisted of 12 ready-made Galfenol sheets with 1.0 mm thickness, 6.0 mm width, and 1.00×10^2 mm length. Every four sheets formed a square hollow rod with a side length of 6.0 mm, as shown in Fig. 15(b). Three sets of rods comprised the magnetostrictive transducer with 1.60×10^6 N/m k_m^I, as shown in Fig. 15(a). Around the material, a steel beam with permanent magnets contributed to the external magnetic field to improve the Villari-Joule effect. Four cylindrical coils connected in tandem were used to induce a current as the magnetic field was varied, as shown in Fig. 15(c). The entire magnetostrictive transducer weighed 0.6 kg, of which the weight of the material component was 0.1 kg. Additional parameters are shown in Table 1.

Fig. 16 shows a schematic of the experimental setup. The excitation point was at the centre of the truss structure. The laser displacement sensors (LK-030, Keyence Corp.) were used to measure the 10th bay of the truss structure. The laser displacement metre data were used to determine the switching signal. An A/D converter was used to capture the metre data from LK-030 and output the switching signal.

4.2. Experimental process of proposed methods

The process of experimental implementation is depicted in Fig. 17 using a flowchart, and can be described as follows:

a) We set up a laser displacement sensor (LK-030, Keyence Corporation) to measure the displacement of the 10th bay node in the X-axis direction. Using the A/D converter, the analog data from the laser displacement sensor were converted to digital data.
b) The timing of the displacement extremum can be detected by the PC programme. Here, according to the proposed control strategies,

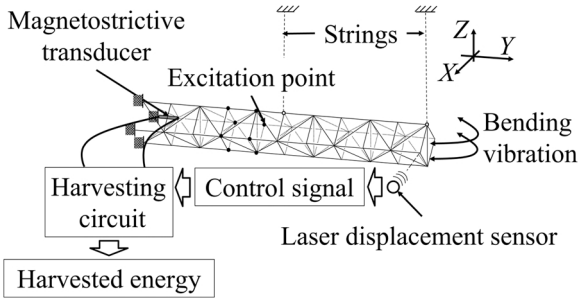

Fig. 16. Experimental setup of truss structure with magnetostrictive transducer.

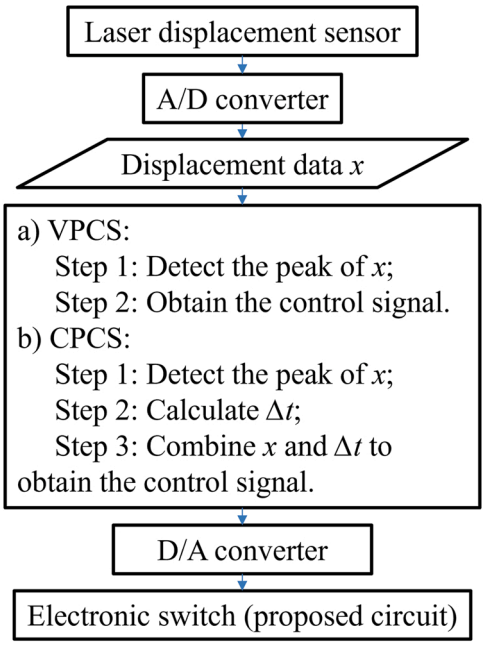

Fig. 17. Experimental implementation process.

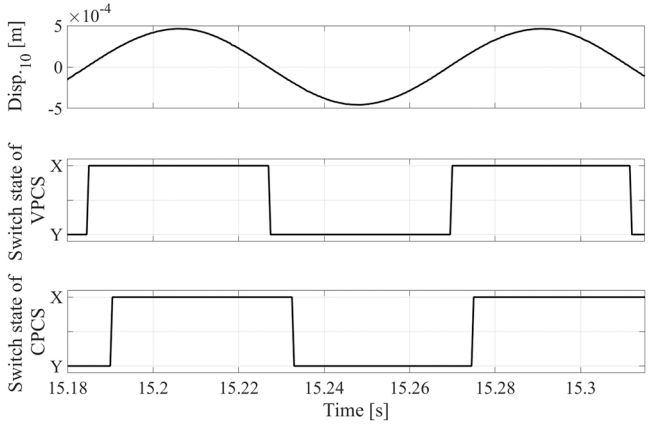

Fig. 18. Time histories of displacement of 10th bay and switching signal for current peak control strategy (CPCS) and voltage peak control strategy (VPCS).

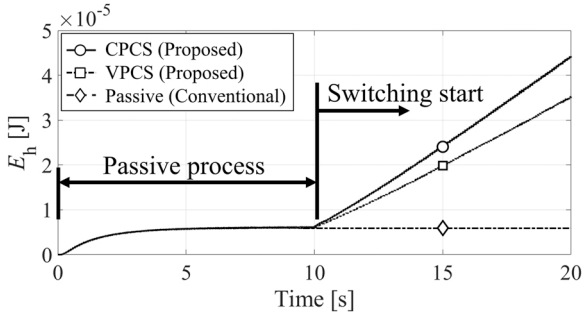

Fig. 19. Time histories of harvested energy (E_h) for passive method, current peak control strategy (CPCS), and voltage peak control strategy (VPCS) obtained from experiments.

displacement data were used to obtain the control signal through the PC programme. We performed VPCS by detecting the displacement extremum. Similarly, we performed CPCS by detecting the displacement extremum and offering Δt, which was calculated from known parameters of the circuit elements.

c) Using the PC programme, we selected the connection of the electronic switch at each moment. These connection data were expressed as control signals.
d) The control signal was converted into a pulse voltage by the A/D converter and output to the electronic switch.
e) The voltage of the harvesting capacitor was measured to evaluate the harvesting performance.

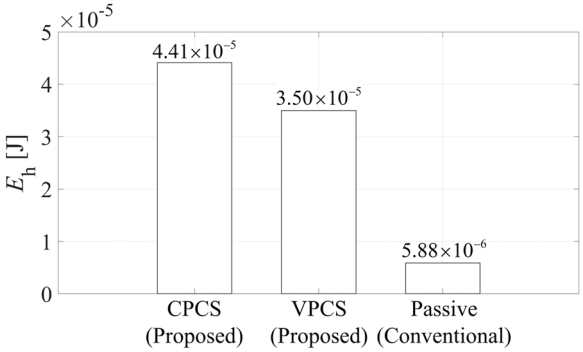

Fig. 20. Harvested energy (E_h) for passive method, current peak control strategy (CPCS), and voltage peak control strategy (VPCS) over 20.0 s obtained from experiments.

4.3. Energy harvesting performance comparison

In the experiments, the excitation direction was along the *X*-axis, as shown in Fig. 16. The truss structure was excited in the bending first natural vibration mode (11.81 Hz). For comparison, the same experiments were conducted using the conventional passive method for 10.0 s and then conducted with VPCS and CPCS for 10.0 s

Fig. 18 shows the time histories of the displacement of the 10th bay and the switching signal obtained using both switching control strategies. The switching frequency was the same as the structural vibration frequency. Meanwhile, compared with the VPCS signal, a fixed phase difference shifted the CPCS signal.

Fig. 19 shows the time histories of the harvested energy obtained using both switching control strategies. As mentioned in section 2.1, the kinetic energy from structural vibrations is converted into electrical energy. The time histories of E_h show that CPCS and VPCS harvest more electrical energy than the passive method and CPCS realises a higher harvesting performance than VPCS.

Lastly, the harvested energy obtained using both switching control strategies is summarised in Fig. 20. We found VPCS and CPCS realise 5.9 and 7.5 times more energy than the passive method, respectively.

5. Conclusion

In this study, two new switching control strategies for energy harvesting that combine a magnetostrictive transducer and electric circuits were proposed. The proposed circuit includes two capacitors, two diodes, and an electronic switch. As a result of the instantaneous switching between points, LC electrical oscillation occurs over a short period. Simultaneously, this short-term LC oscillation increases the voltage across the inverse capacitor to a maximum value, which promotes the continuous transfer of charge to the harvesting capacitor. The proposed method utilises the instantaneous extreme voltages generated by LC electrical oscillations to achieve large-scale and efficient energy harvesting performances. Approximately 45 μJ of energy were harvested over 20 s.

Through numerical simulations, the feasibility and robustness of each proposed switching control strategy were predicted. To validate

their energy harvesting performance, experiments were performed using a cantilevered truss structure. The results showed that the proposed strategies were more effective than the passive method (no switching) with similar robustness. In the experimental environment, CPCS harvested 7.5 times more energy than the conventional passive method. The amount of harvested energy observed in this study was relatively small for use in practical applications, and the switching control strategies can only be used for single-mode vibrations. Nevertheless, they achieved a substantial increase in energy harvesting compared to the passive method without needing to alter the properties of the raw materials involved in the system.

In future work, the switching control strategies will be extended to multimodal vibration conditions. Additionally, a new design for a more efficient and lightweight transducer will be investigated to satisfy the energy supply requirement of the electronic switches and space-constrained application environment.

Funding

The authors received the following financial support for the research, authorship, and/or publication of this article: Grant-in-Aid for Scientific Research (B) (KAKENHI) (grant number 18H01619, 22H01675), Grant-in-Aid for Scientific Research (C) (KAKENHI) (grant number 19K04069), JSPS Core-to-Core Program, A. Advanced Research Networks (JPJSCCA20200005), and JST, the establishment of university fellowships (grant number JPMJFS2102).

CRediT authorship contribution statement

An Li: Conceptualization, Methodology, Validation, Writing – original draft, Funding acquisition. **Keiju Goto:** Methodology, Writing – review & editing. **Yuusuke Kobayashi:** Methodology, Writing – review & editing. **Yushin Hara:** Investigation, Writing – review & editing. **Yu Jia:** Writing – review & editing. **Yu Shi:** Writing – review & editing. **Constantinos Soutis:** Writing – review & editing. **Hiroki Kurita:** Writing – review & editing. **Fumio Narita:** Writing – review & editing, Funding acquisition. **Keisuke Otsuka:** Investigation, Writing – review & editing. **Kanjuro Makihara:** Supervision, Funding acquisition.

Declaration of Competing Interest

The authors declare that they have no known competing financial interests or personal relationships that could have appeared to influence the work reported in this paper.

Data Availability

Data will be made available on request.

Appendix A

In this study, the magnetostrictive transducer was attached in the infrastructure truss structure, as shown in Fig. 7. During horizontal bending vibration, the deformation amplitude at the fixed end of the truss is larger, thus achieving more effective energy harvesting. Compared with the dimensions of the truss structure, the magnetostrictive transducer is a relatively small-size energy converter. When the local dynamics of a magnetostrictive transducer are negligible, the position coordinate vector $\mathbf{x}$ of each node in the global coordinate system is related to the displacement vector $\mathbf{u}_i$ in the i-th local coordinate system via a transformation matrix $\mathbf{H}_i$:

$$\mathbf{u}_i = \mathbf{H}_i\mathbf{x}, \tag{A.1}$$

where $\mathbf{u}_i$ is defined as $[u_k, u_j]^{\mathrm{T}}$, and u_k and u_j represent the positions of the k-th and j-th nodes connected to the i-th bar member, respectively. The axial force P_i applied to the i-th bar member can be described as

$$P_i = k_{ti}\left(u_k - u_j\right), \tag{A.2}$$

where k_{ti} represents the stiffness of the i-th bar member. The potential energy of a bar member can be described as

$$W_{\mathrm{m}i} = (\mathbf{G}\mathbf{H}_i\mathbf{x} - b_{ci}I_i)\frac{k_{ci}}{2}(\mathbf{G}\mathbf{H}_i\mathbf{x} - b_{ci}I_i), \tag{A.3}$$

where

$$k_{ci} \equiv \frac{k^I_{\mathrm{m}i}k_{ti}}{k^I_{\mathrm{m}i} + k_{ti}},\ b_{ci} \equiv \frac{b_{\mathrm{m}i}}{k^I_{\mathrm{m}i}},\ \mathbf{G} = [\,1 \quad -1\,]. \tag{A.4}$$

Here, I_i, $b_{\mathrm{m}i}$, and $k^I_{\mathrm{m}i}$ represent the current, magnetostriction coefficient, and constant-current stiffness of the i-th magnetostrictive material, respectively. The total potential energy W_{total} of the truss structure can be expressed as

$$W_{\mathrm{total}} = \sum_{i=1}^{N_{\mathrm{m}}} W_{\mathrm{m}i} + \sum_{i=N_{\mathrm{m}}+1}^{N_{\mathrm{t}}} W_{ti} = \sum_{i=1}^{N_{\mathrm{m}}}(\mathbf{G}\mathbf{H}_i\mathbf{x} - b_{ci}I_i)\frac{k_{ci}}{2}(\mathbf{G}\mathbf{H}_i\mathbf{x} - b_{ci}I_i) + \sum_{i=N_{\mathrm{m}}+1}^{N_{\mathrm{t}}}(\mathbf{G}\mathbf{H}_i\mathbf{x})\frac{k_{ti}}{2}(\mathbf{G}\mathbf{H}_i\mathbf{x}). \tag{A.5}$$

We suppose that m_l is the mass concentrated at the l-th node. The total kinetic energy T_{total} can then be described as

$$T_{\mathrm{total}} = \sum_{l=1}^{N_{\mathrm{node}}} T_l = \frac{1}{2}\dot{\mathbf{x}}^{\mathrm{T}}\mathbf{M}\dot{\mathbf{x}}, \tag{A.6}$$

where the mass matrix of structure $\mathbf{M}$ is defined as

$$\mathbf{M} \equiv \mathrm{blockdiag}[\,\mathbf{M}_1, \quad \mathbf{M}_2, \quad \cdots \quad , \mathbf{M}_{N_{\mathrm{node}}}\,], \tag{A.7}$$

$$\mathbf{M}_l \equiv \mathrm{diag}[\, m_l, \quad m_l, \quad m_l \,]. \tag{A.8}$$

From Eqs. (A.5) and (A.6), the motion equation for the magnetostrictive transducer can be derived using Hamilton's principle as

$$\mathbf{M}\ddot{\mathbf{x}} + \mathbf{D}\dot{\mathbf{x}} + \mathbf{K}\mathbf{x} = \mathbf{B}_{\mathrm{m}}\mathbf{I} + \mathbf{f}_{\mathrm{ext}}, \tag{A.9}$$

where $\mathbf{x}$ represents the position coordinates of each node; $\mathbf{f}_{\mathrm{ext}}$ is the multiple external force matrix; and $\mathbf{M}$, $\mathbf{D}$, $\mathbf{K}$, $\mathbf{B}_{\mathrm{m}}$, and $\mathbf{I}$ are the mass, damping coefficient, stiffness at constant current, magnetostriction-stiffness composite coefficient, and induced current of magnetostrictive transducer matrices, respectively.

References

[1] G. Park, T. Rosing, M.D. Todd, C.R. Farrar, W. Hodgkiss, Energy harvesting for structural health monitoring sensor networks, J. Infrastruct. Syst. 14 (1) (2008) 64–79, https://doi.org/10.1061/(ASCE)1076-0342(2008)14:1(64).

[2] P. Kamalinejad, C. Mahapatra, Z. Sheng, S. Mirabbasi, V.C. Leung, Y.L. Guan, Wireless energy harvesting for the internet of things, IEEE Commun. Mag. 53 (6) (2015) 102–108, https://doi.org/10.1109/MCOM.2015.7120024.

[3] H. Wang, A. Jasim, X. Chen, Energy harvesting technologies in roadway and bridge for different applications – a comprehensive review, Appl. Energy 212 (2018) 1083–1094, https://doi.org/10.1016/j.apenergy.2017.12.125.

[4] D. Shen, J. Wen, J. Ma, Y. Hu, R. Wang, J. Li, A novel linear inertial piezoelectric actuator based on asymmetric clamping materials, Sens. Actuators A 303 (2020), 111746, https://doi.org/10.1016/j.sna.2019.111746.

[5] Y. Shi, Y. Jia, Multimodal shear wave deicing using fibre piezoelectric actuator on composite for aircraft wings, IEEE/ASME Trans. Mechatron. 23 (5) (2018) 2090–2098, https://doi.org/10.1109/TMECH.2018.2862433.

[6] A. Haroun, C. Lee, Dielectric-elastomer-enhanced triboelectric nanogenerator with amplified outputs, Sens. Actuators A 333 (2022), 113270, https://doi.org/10.1016/j.sna.2021.113270.

[7] S. Khan, Y.S. Pydi, S.S. Mani Prabu, I.A. Palani, P. Singh, Development and actuation analysis of shape memory alloy reinforced composite fin for aerodynamic application, Sens. Actuators A 331 (2021), 113012, https://doi.org/10.1016/j.sna.2021.113012.

[8] S. Kang, S. Cha, Y. Hwang, Y. Lee, S. Choi, Controllable magnetorheological fluid based actuators for 6-degree-of-freedom haptic master applicable to robot-assisted surgery, Sens. Actuators A 279 (2018) 649–662, https://doi.org/10.1016/j.sna.2018.06.057.

[9] M. Verma, V. Lafarga, C. Collette, Perfect collocation using self-sensing electromagnetic actuator: application to vibration control of flexible structures, Sens. Actuators A 313 (2020), 112210, https://doi.org/10.1016/j.sna.2020.112210.

[10] G. Diguet, G. Sebald, M. Nakano, M. Lallart, J. Cavaillé, Analysis of magneto rheological elastomers for energy harvesting systems, Int. J. Appl. Electromagn. Mech. 64 (1–4) (2020) 439–446, https://doi.org/10.3233/JAE-209350.

[11] G. Diguet, G. Sebald, M. Nakano, M. Lallart, J. Cavaillé, Optimization of magneto-rheological elastomers for energy harvesting applications, Smart Mater. Struct. 29 (7) (2020), 075017, https://doi.org/10.1088/1361-665X/ab8837.

[12] H. Kurita, S. Fakhruddin, D. Neyama, K.Y. Inoue, T. Tayama, D. Chiba, M. Watanabe, H. Shiku, F. Narita, Detection of virus-like particles using magnetostrictive vibration energy harvesting, Smart Mater. Struct. 345 (2022), 113814, https://doi.org/10.1016/j.sna.2022.113814.

[13] Z. Deng, M.J. Dapino, Review of magnetostrictive vibration energy harvesters, Smart Mater. Struct. 26 (10) (2017), 103001, https://doi.org/10.1088/1361-665X/aa8347.

[14] H. Liang, G. Hao, O.Z. Olszewski, A review on vibration-based piezoelectric energy harvesting from the aspect of compliant mechanisms, Sens. Actuators A 331 (2021), 112743, https://doi.org/10.1016/j.sna.2021.112743.

[15] G. Lombardi, M. Lallart, Synchronous electric charge and induced current extraction (SECICE): a unified nonlinear technique combining piezoelectric and electromagnetic harvesting, Smart Mater. Struct. 30 (2021), 025029, https://doi.org/10.1088/1361-665X/abd346.

[16] A. Bade, D. Guyomar, E. Lefeuvre, C. Richard, Piezoelectric energy harvesting using a synchronized switch technique, J. Intell. Mater. Syst. Struct. 17 (8–9) (2006) 831–839, https://doi.org/10.1177/1045389X06057533.

[17] Y. Jia, A.A. Seshia, Five topologies of cantilever-based MEMS piezoelectric vibration energy harvesters: a numerical and experimental comparison, Microsyst. Tech. 22 (2016) 2841–2852, https://doi.org/10.1007/s00542-015-2599-z.

[18] Y. Hara, K. Saito, K. Makihara, Compact, digital and self-powered piezoelectric vibration energy harvester with generation control using voltage measurement circuit, Sens. Actuators A 299 (2019), 111609, https://doi.org/10.1016/j.sna.2019.111609.

[19] Y. Hara, Y. Yamamoto, K. Makihara, Self-sensing state estimation of switch-controlled energy harvesters, J. Intell. Mater. Syst. Struct. 31 (20) (2020) 2326–2341, https://doi.org/10.1177/1045389X20943944.

[20] Y. Hara, M. Zhou, A. Li, K. Otsuka, K. Makihara, Piezoelectric energy enhancement strategy for active fuzzy harvester with time-varying and intermittent switching, Smart Mater. Struct. 30 (1) (2021), 015038, https://doi.org/10.1088/1361-665X/abca08.

[21] F. Narita, M. Fox, A review on piezoelectric, magnetostrictive, and magnetoelectric materials and device technologies for energy harvesting applications, Adv. Eng. Mater. 20 (5) (2018), 1700743, https://doi.org/10.1002/adem.201700743.

[22] A.G. Olabi, A. Grunwald, Design and application of magnetostrictive materials, Mater. Des. 29 (2) (2008) 469–483, https://doi.org/10.1016/j.matdes.2006.12.016.

[23] F. Narita, Z. Wang, H. Kurita, Z. Li, Y. Shi, Y. Jia, C. Soutis, A review of piezoelectric and magnetostrictive biosensor materials for detection of COVID-19 and other viruses, Adv. Mater. 33 (1) (2021), 2005448, https://doi.org/10.1002/adma.202005448.

[24] C.S. Clemente, D. Davino, G. Maddaloni, M.R. Pecce, C. Visone, A magnetostrictive energy harvesting system for bridge structural health monitoring, Adv. Sci. Technol. 101 (2016) 20–25, https://doi.org/10.4028/www.scientific.net/AST.101.20.

[25] A. Viola, V. Franzitta, G. Cipriani, V. Di Dio, F.M. Raimondi, M. Trapanese, A magnetostrictive electric power generator for energy harvesting from traffic: design and experimental verification, IEEE Trans. Magn. 51 (11) (2015), 8208404, https://doi.org/10.1109/TMAG.2015.2454442.

[26] M. Zucca, A. Hadadian, O. Bottauscio, Quantities affecting the behavior of vibrational magnetostrictive transducers, IEEE Trans. Magn. 51 (1) (2015), 8000104, https://doi.org/10.1109/TMAG.2014.2359248.

[27] K. Mori, T. Horibe, S. Ishikawa, Y. Shindo, F. Narita, Characteristics of vibration energy harvesting using giant magnetostrictive cantilevers with resonant tuning, Smart Mater. Struct. 24 (12) (2015), 125032, https://doi.org/10.1088/0964-1726/24/12/125032.

[28] A.E. Clark, K.B. Hathaway, M. Wun-Fogle, J.B. Restorff, T.A. Lograsso, V. M. Kepppens, G. Petculescu, R.A. Taylor, Extraordinary magnetoelectricity and lattice softening in Bcc Fe-Ga alloys, J. Appl. Phys. 93 (10) (2003) 8621–8623, https://doi.org/10.1063/1.1540130.

[29] M. Wun-Fogle, J.B. Restorff, A.E. Clark, Soft and hard elastic moduli of galfenol transduction, Elem., J. Appl. Phys. 105 (7) (2009) 07A923, https://doi.org/10.1063/1.3058645.

[30] G. Petculescu, K.B. Hathaway, T.A. Lograsso, M. Wun-Fogle, A.E. Clark, Magnetic field dependence of galfenol elastic properties, J. Appl. Phys. 97 (10) (2005) 10M315, https://doi.org/10.1063/1.1855711.

[31] S. Kita, T. Ueno, S. Yamada, Improvement of force factor of magnetostrictive vibration power generator for high efficiency, J. Appl. Phys. 117 (17) (2015) 17B508, https://doi.org/10.1063/1.4907237.

[32] T. Ueno, Magnetostrictive vibrational power generator for battery-free IoT application, AIP Adv. 9 (3) (2019), 035018, https://doi.org/10.1063/1.5079882.

[33] M. Li, Y. Wen, P. Li, J. Yang, X. Dai, A rotation energy harvester employing cantilever beam and magnetostrictive/piezoelectric laminate transducer, Sens. Actuators A 166 (1) (2011) 102–110, https://doi.org/10.1016/j.sna.2010.12.026.

[34] P. Li, Y. Wen, C. Jia, X. Li, A magnetoelectric composite energy harvester and power management circuit, IEEE Trans. Ind. Electron. 58 (7) (2011) 2944–2951, https://doi.org/10.1109/TIE.2010.2076308.

[35] I. Iannone, C.S. Clemente, D. Davino, V.P. Loschiavo, AC-DC Boost Modelling for Magnetostrictive Energy Harvesting, 2021 IEEE International Conference on Environment and Electrical Engineering and 2021 IEEE Industrial and Commercial Power Systems Europe (EEEIC / I&CPS Europe), 2021, 1–6. https://doi.org/10.1109/EEEIC/ICPSEurope51590.2021.9584550.

[36] C.S. Clemente, D. Davino, I. Iannone, V.P. Loschiavo, Experimental Verification of an AC-DC Boost towards Non-Periodic (AC) Energy Harvesting, 2022 IEEE 21st Mediterranean Electrotechnical Conference (MELECON), 2021. https://doi.org/10.1109/MELECON53508.2022.9843055.

An Li received the bachelor degree in Mechanical Engineering from Tianjin University, Tianjin, China, in 2016 and the master degree in Department of Aerospace Engineering from Tohoku University, Sendai, Japan in 2021. His research focuses on energy harvesting and vibration suppression.

Keiju Goto received a bachelor's degree in mechanical engineering from Kanazawa University in 2021 and a master's degree in aerospace engineering from Tohoku University in 2023. His research focuses on control of flexible robot arm and energy harvesting with magnetostrictive transducer.

Yuusuke Kobayashi received the bachelor's degree in Mechanical Engineering from Nihon University in 2022. His research focuses on vibration suppression and energy harvesting with magnetostrictive transducer.

Yushin Hara received his bachelor degree in 2017, master degree in 2019 from Department of Aerospace Engineering, Tohoku University. He has been an Ph.D. candidate at Tohoku University. His current research interests involve self-powered energy-harvesting, semi-active vibration suppression, self-sensing, and system identification.

Dr Yu Jia is a Senior Lecturer in Mechanical Engineering at Aston University, having previously been an Associate Professor at University of Chester. He graduated PhD in Engineering from University of Cambridge and Masters of Electromechanical Engineering from University of Southampton. His research interests are on energy harvesting, nonlinear dynamics, smart systems, and multifunctional materials. He has published over a hundred academic papers, has secured over £ 3 M in external research funding, is a co-founder of 8power Ltd, and is a Senior Member of the IEEE.

Prof Yu Shi is a Professor of smart composite materials for multifunctionalities of composites with embedded electronics for monitoring, communication and energy harvesting etc. In addition, he also investigated the multiphysics composite modelling and manufacturing and sustainability of composite materials. He has been working with industries, academics and research organisation with totally funded project up to £ 8.5 M for aerostructure, automotive, sustainable energy and healthcare.

Constantinos Soutis PhD(Cantab), FREng is Professor Emeritus of Aerospace Engineering at the University of Manchester (UK). His research focuses on damage mechanics of heterogeneous anisotropic composite material systems and structural health monitoring. He has authored or co-authored more than 400 ISI listed papers and successfully supervised over 40 PhD students. He is a Chartered Engineer and a Fellow of the UK Royal Academy of Engineering. The Academy's Fellows represent the nation's best engineering researchers, innovators, entrepreneurs, business and industry leaders.

Hiroki Kurita has been Assistant Professor at Tohoku University in Japan since 2018. He thinks it is possible to develop materials with high magnetostrictive properties, energy harvesting performance, and mechanical properties by designing the structure using additive manufacturing. He addresses optimizing the fabrication parameters for laser powder additive manufacturing of magnetostrictive alloys and designing stress-concentrated structures to dramatically increase their energy harvesting performance.

Fumio Narita is currently a professor at the Department of Frontier Sciences for Advanced Environment at Tohoku University in Japan. He is engaged in research to design and develop piezoelectric/magnetostrictive materials and structures in energy harvesting and self-powered environmental monitoring. He extensively uses state-of-the-art electro-magneto–mechanical characterization techniques in combination with computational multiscale modeling to understand the fundamental structure–property relationships of complex multifunctional composite materials.

Keisuke Otsuka received his bachelor degree in 2014, master degree in 2016, Ph.D. degree in 2020 from Department of Aerospace Engineering, Tohoku University. He has been an assistant professor at Tohoku University since 2020. In 2015, he studied aerodynamics at KTH Royal Institute of Technology, Sweden. In 2019, he engaged in the flexible aircraft research in the load control and aeroelastics laboratory at Imperial College London, U.K. as a visiting research student. His research interests are multibody dynamics and aeroelasticity.

Kanjuro Makihara, Doctor of Engineering, received his Bachelor's degree in Aeronautics and Astronautics from the University of Tokyo in 1998 and completed his Ph.D. program from the Graduate School of the University of Tokyo in 2004. Since 2004, he has been an Aerospace Project Research Associate at JAXA/ISAS and has devoted himself to energy-recycling vibration suppression for space structures. After serving as a visiting researcher at the University of Cambridge, U.K., he has been working as an Associate Professor of Aerospace Engineering at the Tohoku University since 2011, and in 2019, he became a professor at the Tohoku University. His current research interests involve semi-active vibration suppression, self-powered energy-harvesting, dynamics of flexible structures, and issues pertaining to space debris.